

Background Subtraction with Drift Correction for Bistatic Radar Reflectivity Measurements

Alexander Ihlow^{*†}, Marius Schmidt^{*†}, Carsten Andrich^{*†}, Reiner S. Thomä^{*†}

^{*}Institute of Information Technology, Technische Universität Ilmenau, Ilmenau, Germany

[†]Thuringian Center of Innovation in Mobility, Ilmenau, Germany

{alexander.ihlow, marius.schmidt, carsten.andrich, reiner.thomae}@tu-ilmenau.de

Abstract—Fundamental research on bistatic radar reflectivity is highly relevant, e.g., to the upcoming mobile communication standard 6G, which includes integrated sensing and communication (ISAC). We introduce a model for correcting instrumentation drift during bistatic radar measurements in anechoic chambers. Usually, background subtraction is applied with the goal to yield the target reflection signal as best as possible while coherently subtracting all signals which were present in both the foreground and background measurement. However, even slight incoherences between the foreground and background measurement process deteriorate the result. We analyze these effects in real measurements in the frequency range 2–18 GHz, taken with the *Bistatic Radar* (BIRA) measurement facility at TU Ilmenau. Applying our proposed drift correction model, we demonstrate up to 40 dB improvement for the removal of direct line-of-sight antenna crosstalk over the state of the art.

Index Terms—Bistatic radar, radar measurements, radar reflectivity, anechoic chambers, network analyzers

I. INTRODUCTION

Measuring target reflection signals from radar targets in anechoic chambers requires major investments in the facility itself as well as high effort in planning, conducting and evaluating the experiments. The target reflection signal is several magnitudes weaker than the illumination signal and often in the order of magnitude of (practically unavoidable) parasitic reflections from the chamber. Therefore, usually background subtraction is applied to yield the target reflection signal as best as possible.

The measurement process is divided into two steps: target measurement and background measurement, i.e., all bistatic transmitter (Tx) and receiver (Rx) constellations have to be taken twice: with and without the target [1]. Several hours may elapse for a measurement, and parameters which were initially presumed as time-invariant may have slightly changed, caused by instrument drift and parasitic effects from cabling due to recurrent bending (for antenna positioning) and temperature changes. As a consequence, the coherence of the background subtraction is limited.

Wideband measurements enable signal resolution in time-domain. Depending on the used bandwidth and the propagation delays, the antenna crosstalk (also termed direct path leakage signal or direct signal interference [2]), the target reflection signal, as well as parasitic reflections can be distinguished.

While in the monostatic and bistatic case target detection and ranging is possible by reflected signals, the forward

scattering case places special challenges, as the signal scattered from a target is received as a modulation on top of the direct path signal [3], [4].

Looking at the state of the art, much work has been done on direct signal interference and clutter cancellation for operational radar systems. A special case are radar reflectivity measurements in anechoic chambers, which we address in this paper. Here, typical measurement times of several hours and frequently bending of RF cabling due to antenna movements induce drift effects that call for special attention in the data postprocessing. For such measurements, coherent background subtraction, first practically demonstrated in [1], is valued as a convenient method for yielding a purified target signal, eliminating antenna crosstalk and parasitic reflections, as long as coherence between foreground and background measurement is ensured. As the main goal is to overcome the phase coherence problems that appear with increasing frequency between multiple measurements, suggested solutions range from improving measurement conditions [5] to various computational methods including image edit- and mean subtraction [6], or principal component analysis [7]. Typically, coherent background subtraction is used and also recommended by IEEE Std 1502 [8, pp. 31 ff.].

The objective of this paper is to model and correct drift effects, improving the coherence of background subtraction. It is organized as follows: Sec. II introduces a long-term measurement, from which actual drift effects can be quantified. Sec. III derives a correction model and applies it on these measurements. Sec. IV shows further results on a multi-position long-term measurement, and Sec. V on a sphere measurement before Sec. VI concludes the paper.

II. DRIFT MEASUREMENT

To analyze the consequences of measurement inaccuracies on background subtraction, focusing on drift, we conducted a long-term measurement of a static scenario in the *Bistatic Radar* (BIRA) measurement facility [9] at TU Ilmenau with the parameters given in Table I.

Treating the first measurement as reference, deviations in phase and amplitude are obvious in Fig. 1 and Fig. 2, increasing with measurement time. The corresponding impulse responses are drawn in Fig. 3. To evaluate drift effects on the performance of background subtraction, we use the first measurement as background, while all other measurements

TABLE I
PARAMETERS OF STATIC LONG-TERM MEASUREMENT.

antenna constellation	Tx: fixed, Rx: fixed
bistatic angle β	antennas facing each other, $\beta = 180^\circ$
radar target	none (direct line-of-sight scenario)
instrument	Keysight N5222B/Option 401 (VNA)
RF connection	Low-loss coaxial RF cables
frequency range	2 ... 18 GHz
frequency spacing	10 MHz
measurement runs	6500
measurement time	18 h

are treated as foreground. The resulting impulse responses after conventional background subtraction are plotted in Fig. 4, showing a peak residue of -20 dB. The goal is to develop a model to reduce these residues.

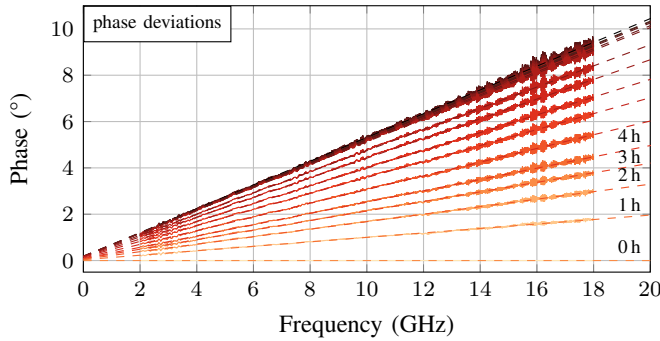


Fig. 1. Phase deviations in static long-term measurement.

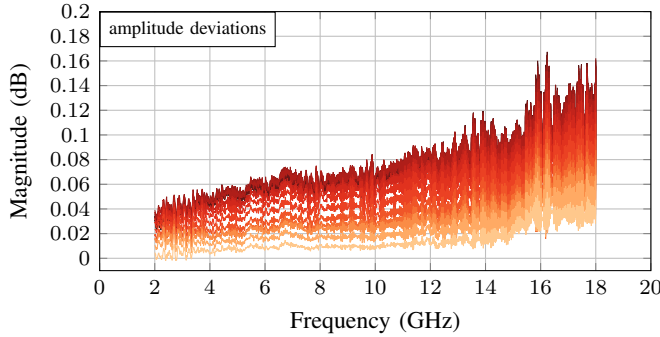


Fig. 2. Amplitude deviations in static long-term measurement.

III. CORRECTION MODEL

From Fig. 1 and Fig. 2 it is obvious that the correction model should consider phase as well as amplitude deviations. Furthermore, it should be able to focus on particular samples of the impulse response, such as the peak from the direct signal (cf. Fig. 3). We formulate the model as follows:

$$\arg \min_{a, b, \varepsilon \in \mathbb{R}} \sum_n \left| \text{IDFT}\{(a + b f) e^{-j \varepsilon f} \mathbf{Z}_{\text{fg}}\}[n] - \mathbf{z}_{\text{bg}}[n] \right|^2 = \quad (1)$$

$$\arg \min_{a, b, \varepsilon \in \mathbb{R}} \sum_n \left| \frac{1}{N} \sum_{k=0}^{N-1} (a + b f_k) e^{-j \varepsilon f_k} \mathbf{Z}_{\text{fg}}[k] e^{j 2 \pi \frac{k}{N} n} - \mathbf{z}_{\text{bg}}[n] \right|^2$$

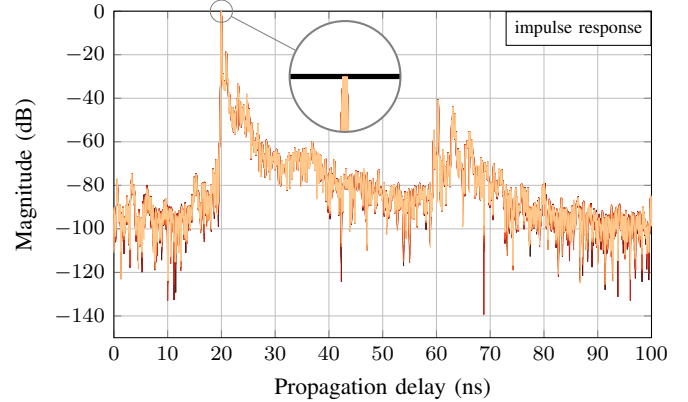


Fig. 3. Impulse responses of static long-term measurement. The set of curves correspond to Fig. 1 and Fig. 2 (cf. the annotation of measurement time in Fig. 1).

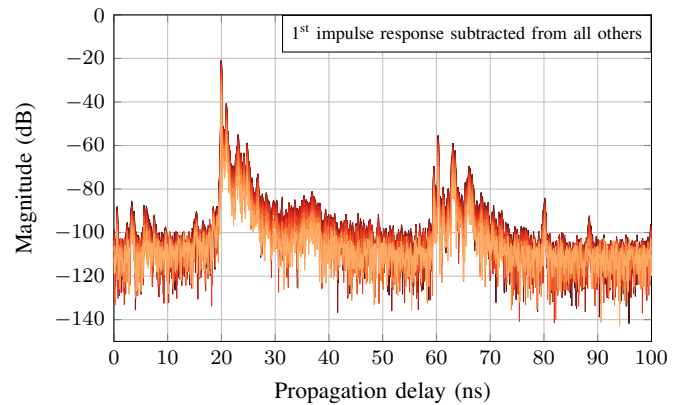


Fig. 4. Impulse responses after conventional background subtraction (without correction): The first measurement is treated as “background” and subtracted from all other measurements. The set of curves correspond to Fig. 1 and Fig. 2 (cf. the annotation of measurement time in Fig. 1).

\mathbf{Z}_{fg} is the spectrum of a single foreground measurement, $\mathbf{z}_{\text{bg}} = \text{IDFT}\{\mathbf{Z}_{\text{bg}}\}$ is the corresponding (same illumination and observation angles and polarization) background measurement in time-domain after inverse discrete Fourier transform (IDFT). The operation $[n]$ selects the relevant samples in time domain, on which the parameter optimization is performed. Of course, all vector multiplications within the $\text{IDFT}\{\cdot\}$ in (1) are *element-wise* products. The commonly used symbol \odot is omitted throughout the paper for better readability.

The frequencies f_k can be defined, e.g., in complex baseband or as physical frequencies. Without loss of generality, we chose $f_k = f_{\text{start}} + (f_{\text{end}} - f_{\text{start}}) \frac{k}{N} (1 + \frac{1}{N})$. In our measurements, $f_{\text{start}} = 2$ GHz, $f_{\text{end}} = 18$ GHz, and $N = 1601$. Doing so, the parameter ε gets the unit $^\circ/\text{GHz}$, b gets the unit $1/\text{GHz}$, a is dimensionless. Note that the choice to apply the correction on the foreground measurement is arbitrary, the model would work also vice versa.

For this model, the partial derivatives can be analytically derived (given in the Appendix), making it easily applicable for numerical solution via, e.g., Newton-Conjugate-Gradient.

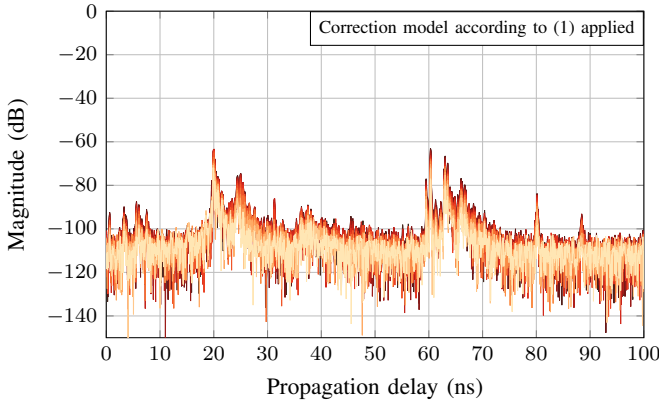


Fig. 5. Impulse responses after background subtraction **with** correction: The first measurement is treated as “background” and subtracted from all other measurements. The model according to (1) is applied, correcting phase and amplitude deviations. This results in an improvement of up to 40 dB regarding peak subtraction.

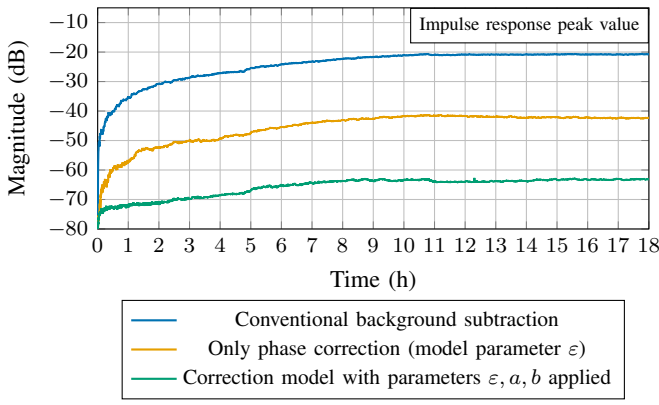


Fig. 6. Performance of background subtraction over all static measurement runs (cf. Table I). The first measurement is treated as “background”. The proposed correction model gains up to 40 dB peak improvement compared to conventional background subtraction.

Applying the correction model onto the longterm measurement, the peak residue reduces from -20 dB to -60 dB, as seen in comparison of Fig. 4 and Fig. 5. Details on peak reduction over time are drawn in Fig. 6, estimated parameters are given in Fig. 7.

IV. MULTI-POSITION MEASUREMENT

To confirm the effectiveness of this algorithm for more realistic scenarios, we conducted a further measurement with parameters according to Table II.

TABLE II
PARAMETERS OF MULTI-POSITION LONG-TERM MEASUREMENT.

RF parameters	same as in Table I
antenna constellation	Tx: fixed, Rx: variable elevation
bistatic angles β	15 constellations between 30° and 150°
radar target	none (direct line-of-sight scenario)
measurement runs	288 for each bistatic angle
measurement time	20 h

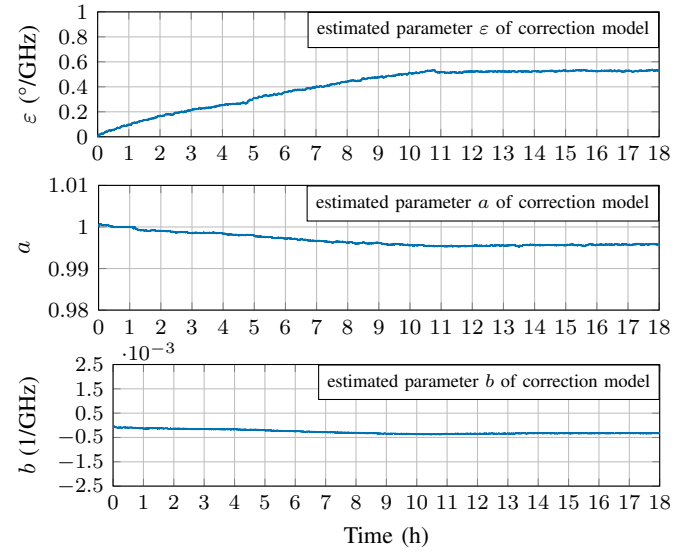


Fig. 7. Estimated parameters for static measurement (cf. Table I).

As these data are too comprehensive to be fully evaluated in this paper, we focus on one representative constellation with the bistatic angle $\beta = 150^\circ$. Fig. 8 and Fig. 9 show further effects not found in the previously analyzed static data, where neither cable bending nor possibly tiny oscillation residues from the gantry arm antenna positioner played a role. Nevertheless, on these data the correction model provides up to 37 dB peak improvement in background subtraction.

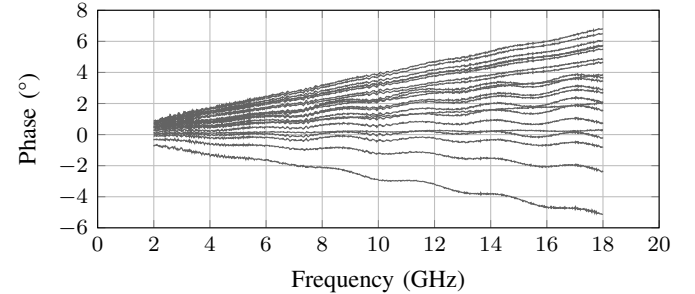


Fig. 8. Phase deviations in multi-position long-term measurement. A clear dependency of the deviations on measurement time, as in Fig. 1 cannot be deduced. However, harmonic phase modulations appear, which are induced by residual mechanical oscillations of the gantry arm antenna positioner.

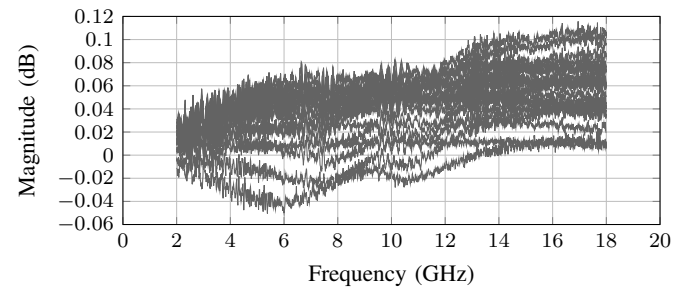


Fig. 9. Amplitude deviations in multi-position long-term measurement.

V. APPLICATION ONTO SPHERE MEASUREMENTS

We applied the proposed algorithm onto measurements of an azimuth cut of a 30 cm sphere in horizontal co-polarization (described in [9] and summarized in Table III).

TABLE III
PARAMETERS OF SPHERE MEASUREMENT.

RF parameters	same as in Table I
antenna constellation	Tx: variable azimuth, Rx: fixed
bistatic angles β	$\beta = 10^\circ \dots 243^\circ$ in 1° azimuth steps
radar target	30 cm sphere
measurement time	1 h 20 min foreground + 1 h 20 min background

As stated in Sec. III, each corresponding pair (same illumination and observation angles as well as polarization) of foreground and background measurement is corrected according to (1). The selected samples n in time domain for which the parameter optimization is performed, are the respective direct signal peak samples within the impulse response of the background measurement, found by $\arg \max_{n \in 0 \dots N-1} \{|\mathbf{z}_{\text{bg}}[n]|\}$.

Results are drawn in Fig. 10 and Fig. 11. The algorithm works well in the bistatic region, removing the residue of the direct path leakage signal. However, in the forward scattering region ($\beta \approx 160^\circ \dots 200^\circ$), where the direct line-of-sight antenna crosstalk can no longer be distinguished from target signals, it is not applicable. Here, the model parameters deviate far from plausible values (cf. Fig. 11), distorting the correctness of estimated bistatic radar reflectivity values.

VI. CONCLUSION

We investigated instrument drift in bistatic radar reflectivity measurements in the BIRA measurement facility [9] at TU Ilmenau. As expected, technically unavoidable deviations in phase and amplitude limit the coherence between foreground and background measurement, even with cutting-edge hardware. This manifests mainly as a residue of the direct signal (line-of-sight antenna crosstalk) after background subtraction. To improve the coherence, we introduced a parametric correction model, containing a phase term and an amplitude term. Model parameter estimation is performed for all corresponding pairs of foreground and background measurements by focusing on the direct line-of-sight signal portion of the impulse responses. Newton-Conjugate-Gradient ensures fast convergence, using the analytically expressed partial derivatives. Regarding direct signal suppression, our algorithm yields up to 40 dB improvement compared to conventional background subtraction. The model is applicable in angular constellations where the direct antenna crosstalk can be distinguished from all target interaction signals in time domain, which is the monostatic and bistatic region. In the forward scattering region, where this demand is not met, conventional background subtraction can be applied.

Whether an interpolation of estimated parameters from the monostatic and bistatic region could be relied upon in the forward scattering region is subject of further investigation.

APPENDIX

To find the minimum of the function

$$\sum_n |\text{IDFT}\{(a + b \mathbf{f}) e^{-j\varepsilon f} \mathbf{Z}_{\text{fg}}\}[n] - \mathbf{z}_{\text{bg}}[n]|^2 = \sum_n |\kappa|^2 \\ = \sum_n \left| \frac{1}{N} \sum_{k=0}^{N-1} (a + b f_k) e^{-j\varepsilon f_k} \mathbf{Z}_{\text{fg}}[k] e^{j2\pi \frac{k}{N} n} - \mathbf{z}_{\text{bg}}[n] \right|^2 \quad (2)$$

with respect to the parameters $\varepsilon, a, b \in \mathbb{R}$, we use $|\kappa|^2 = \Re\{\kappa\}^2 + \Im\{\kappa\}^2$ with $\kappa \in \mathbb{C}$. To express the first and second derivatives in general, we use the chain rule and $p, \nu \in \mathbb{R}$:

$$\frac{\partial |\kappa|^2}{\partial p} = 2 \Re\{\kappa\} \frac{\partial}{\partial p} \Re\{\kappa\} + 2 \Im\{\kappa\} \frac{\partial}{\partial p} \Im\{\kappa\} \quad (3)$$

$$\frac{\partial^2 |\kappa|^2}{\partial p \partial \nu} = 2 \frac{\partial}{\partial \nu} \Re\{\kappa\} \frac{\partial}{\partial p} \Re\{\kappa\} + 2 \Re\{\kappa\} \frac{\partial^2}{\partial p \partial \nu} \Re\{\kappa\} \\ + 2 \frac{\partial}{\partial \nu} \Im\{\kappa\} \frac{\partial}{\partial p} \Im\{\kappa\} + 2 \Im\{\kappa\} \frac{\partial^2}{\partial p \partial \nu} \Im\{\kappa\} \quad (4)$$

Explicitly, the first and second derivatives in (3) and (4) are:

$$\frac{\partial}{\partial \varepsilon} [\kappa] = \frac{1}{N} \sum_{k=0}^{N-1} (a + b f_k) (-j f_k) e^{-j\varepsilon f_k} \mathbf{Z}_{\text{fg}}[k] e^{j2\pi \frac{k}{N} n} \\ = \text{IDFT}\{(a + b \mathbf{f}) (-j \mathbf{f}) e^{-j\varepsilon f} \mathbf{Z}_{\text{fg}}\} \quad (5)$$

$$\frac{\partial}{\partial a} [\kappa] = \frac{1}{N} \sum_{k=0}^{N-1} e^{-j\varepsilon f_k} \mathbf{Z}_{\text{fg}}[k] e^{j2\pi \frac{k}{N} n} \\ = \text{IDFT}\{e^{-j\varepsilon f} \mathbf{Z}_{\text{fg}}\} \quad (6)$$

$$\frac{\partial}{\partial b} [\kappa] = \frac{1}{N} \sum_{k=0}^{N-1} f_k e^{-j\varepsilon f_k} \mathbf{Z}_{\text{fg}}[k] e^{j2\pi \frac{k}{N} n} \\ = \text{IDFT}\{\mathbf{f} e^{-j\varepsilon f} \mathbf{Z}_{\text{fg}}\} \quad (7)$$

$$\frac{\partial^2}{\partial \varepsilon^2} [\kappa] = \frac{1}{N} \sum_{k=0}^{N-1} (a + b f_k) (-f_k^2) e^{-j\varepsilon f_k} \mathbf{Z}_{\text{fg}}[k] e^{j2\pi \frac{k}{N} n} \\ = \text{IDFT}\{(a + b \mathbf{f}) (-\mathbf{f}^2) e^{-j\varepsilon f} \mathbf{Z}_{\text{fg}}\} \quad (8)$$

$$\frac{\partial^2}{\partial a \partial \varepsilon} [\kappa] = \frac{1}{N} \sum_{k=0}^{N-1} (-j f_k) e^{-j\varepsilon f_k} \mathbf{Z}_{\text{fg}}[k] e^{j2\pi \frac{k}{N} n} \\ = \text{IDFT}\{-j \mathbf{f} e^{-j\varepsilon f} \mathbf{Z}_{\text{fg}}\} \quad (9)$$

$$\frac{\partial^2}{\partial \varepsilon \partial b} [\kappa] = \frac{1}{N} \sum_{k=0}^{N-1} (-j f_k^2) e^{-j\varepsilon f_k} \mathbf{Z}_{\text{fg}}[k] e^{j2\pi \frac{k}{N} n} \\ = \text{IDFT}\{-j \mathbf{f}^2 e^{-j\varepsilon f} \mathbf{Z}_{\text{fg}}\} \quad (10)$$

$$\frac{\partial^2}{\partial a^2} [\kappa] = \frac{\partial^2}{\partial b^2} [\kappa] = \frac{\partial^2}{\partial b \partial a} [\kappa] = \frac{\partial^2}{\partial a \partial b} [\kappa] = 0 \quad (11)$$

With these expressions it is straightforward to find the minimum, e.g., with the Newton-Conjugate-Gradient algorithm.

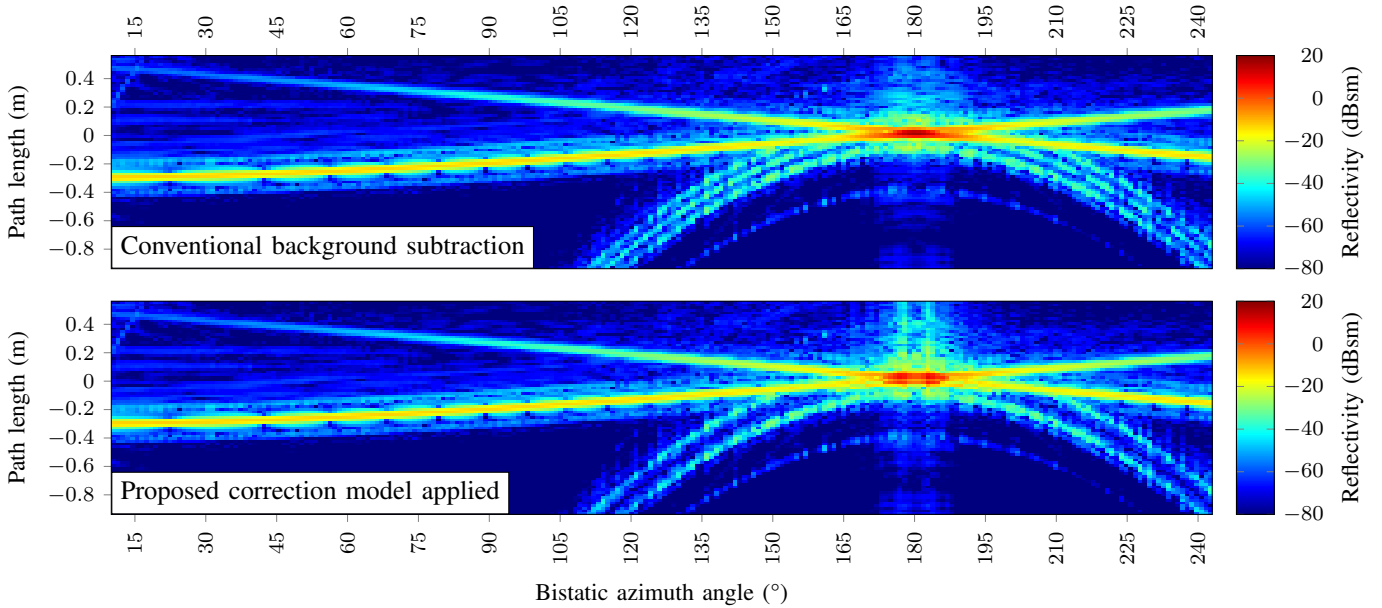


Fig. 10. Bistatic azimuth cut of a 30 cm sphere, measured in the BIRA facility from 2 to 18 GHz, horizontal to horizontal (HH) polarization. Top plot with conventional background subtraction (foreground – background), bottom plot with the proposed correction model according to (1) applied.

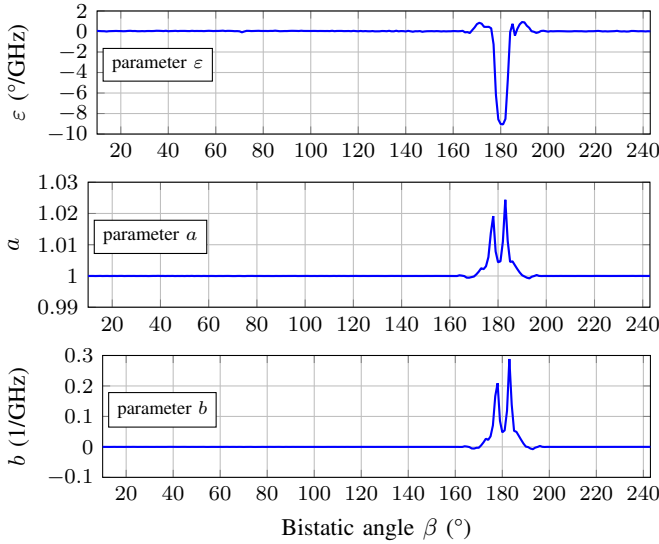


Fig. 11. Estimated model parameters on sphere measurements. In the pseudo-monostatic and bistatic region, the model shows valid results. In the forward scattering region ($\beta \approx 160$ – 200 °), the model is not applicable as the direct line-of-sight antenna crosstalk is no longer distinguishable from target interaction signals in the impulse responses. Here, the model parameters deviate far from plausible values, cf. Fig. 7.

REFERENCE IMPLEMENTATION OF THE ALGORITHM

A reference implementation in the Python programming language of the core function containing the proposed model and optimization is published on arxiv.org.

ACKNOWLEDGMENT

The research was funded by the Federal State of Thuringia, Germany, and the European Social Fund (ESF) under grants

2017 FGI 0007 (project “BiRa”), 2021 FGI 0007 (project “Kreatör”), and 2023 IZN 0005 (project “research initiative digital mobility”). We thank Dr. Tobias Nowack for supporting the measurements and Lisa Hickl for reviewing the math.

REFERENCES

- [1] P. Fritsch and F. Heart, “A new method of measuring small radar cross sections by digital vector-field subtraction,” *Proceedings of the IEEE*, vol. 52, pp. 628–629, May 1964, doi: 10.1109/PROC.1964.3027.
- [2] J. L. Garry, C. J. Baker, and G. E. Smith, “Evaluation of direct signal suppression for passive radar,” *IEEE Transactions on Geoscience and Remote Sensing*, vol. 55, pp. 3786–3799, Jul. 2017, doi: 10.1109/TGRS.2017.2680321.
- [3] J. I. Glaser, “Bistatic RCS of complex objects near forward scatter,” *IEEE Transactions on Aerospace and Electronic Systems*, vol. AES-21, pp. 70–78, Jan. 1985, doi: 10.1109/TAES.1985.310540.
- [4] M. Gashinova1, L. Daniel, E. Hoare, V. Sizov, K. Kabakchiev, and M. Cherniakov, “Signal characterisation and processing in the forward scatter mode of bistatic passive coherent location systems,” *EURASIP Journal on Advances in Signal Processing*, vol. 36, pp. 1–13, Dec. 2013, doi: 10.1186/1687-6180-2013-36.
- [5] R. E. Jarvis, J. G. Metcalf, J. E. Ruyle, and J. W. McDaniel, “Wideband measurement techniques for extracting accurate RCS of single and distributed targets,” *IEEE Transactions on Instrumentation and Measurement*, vol. 71, pp. 1–12, 2022, doi: 10.1109/TIM.2022.3152237.
- [6] A. Bati, L. To, and D. Hilliard, “Advanced radar cross section clutter removal algorithms,” in *Fourth European Conference on Antennas and Propagation*, Barcelona, Spain, Jul. 2010. [Online]. Available: <https://ieeexplore.ieee.org/document/5505008>
- [7] P. O. Leye, A. Banelli, S. Aldhaheri, C. Kasmi, F. Vega, and I. Yahi, “Background and clutter removal algorithm for RCS extraction in semi-anechoic chamber,” in *Antenna Measurement Techniques Association Symposium (AMTA)*, Denver, CO, USA, Oct. 2023, pp. 1–5, doi: 10.23919/AMTA58553.2023.10293426.
- [8] “IEEE Recommended Practice for Radar Cross-Section Test Procedures,” *IEEE Std 1502-2020 (Revision of IEEE Std 1502-2007)*, pp. 1–78, 2020, doi: 10.1109/IEEEESTD.2020.9310748.
- [9] C. Andrich, T. F. Nowack, A. Ihlow, S. Giehl, M. Engelhardt, G. Sommerkorn, A. Schwind, W. Hofmann, C. Bornkessel, M. A. Hein, and R. S. Thomä, “BIRA: A Spherical Bistatic Radar Reflectivity Measurement System,” 2025, arXiv:2407.13749 [eess.SP].